JOURNAL OF MATERIALS SCIENCE 27 (1992) 146–152

Contact thermal shock test of ceramics

W. P. ROGERS
Department of Mechanical Engineering, CB-427, University of Colorado, Boulder, CO 80309, USA

A. F. EMERY
Department of Mechanical Engineering, FU-10, University of Washington, Seattle, WA 98195, USA

A novel quantitative thermal shock test of ceramics is described. The technique employs contact between a metal cooling rod and hot disc-shaped specimen. In contrast with traditional techniques, the well-defined thermal boundary condition allows for accurate analyses of heat transfer, stress, and fracture. Uniform equi-biaxial tensile stresses are induced in the centre of the test specimen. Transient specimen temperature and acoustic emission are monitored continuously during the thermal stress cycle. The technique is demonstrated with soda-lime glass specimens. Experimental results are compared with theoretical predictions based on a finite element method thermal stress analysis combined with a statistical model of fracture. Material strength parameters are determined using concentric ring flexure tests. Good agreement is found between experimental results and theoretical predictions of failure probability as a function of time and initial specimen temperature.

1. Introduction

A number of thermal shock tests have been used to evaluate the reliability of ceramic materials subjected to rapid temperature change. The procedure for most thermal shock tests involves heating a group of rod-shaped specimens to a specified temperature, quenching them by immersion in a fluid medium (most often water), followed by measurements of retained strength (most often using three or four point bending) [1–3]. The minimum temperature difference (between the initial specimen temperature and the quenching medium temperature) which causes a significant decrease in the retained strength of the specimens, known as the critical temperature difference, is a measure of the thermal shock resistance of the material [4]. The long history and simplicity of the water quench test have led to its continued widespread use. Unfortunately, a number of problems with this technique have been identified over the past ten years. Results have been found to depend on the quenching medium [5], the bath temperature [6], and the specimen size [7]. Small variations in the test procedure can cause large variations in results [8]. Moreover, groups of experimental data frequently conflict with one another and do not agree well with theory [9, 10].

Many of the difficulties with quench tests can be traced to the lack of an accurate model of the heat transfer conditions. Boiling phenomena (which are sensitive to the quenching medium, bath temperature, and specimen surface roughness) cause the convection heat transfer coefficient to vary by several orders of magnitude during the thermal shock cycle. The complexity of these boiling effects prevents accurate analysis of the thermal stress. An additional problem with the water quench test is that the critical temperature difference is not a reliable indicator of the onset of thermal shock fracture. Damage is likely to occur at temperatures well below the critical temperature difference as determined by a measurable decrease in retained strength [11]. Residual stresses are common following a thermal shock and can have a large effect on the retained strength. Indeed, oil quenching is a well known technique used to strengthen glass. Retained strength also depends most directly on the depth of thermal shock crack propagation which in turn depends on the thermal stress state and specimen geometry.

More recently, other thermal shock tests have been developed in order to overcome the problems of the traditional water quench test. The air jet technique [12, 13] uses a controlled jet of air to cool the surface of a disc-shaped ceramic specimen. The heat transfer conditions are modelled with a constant convection boundary condition over the centre of the disc. One drawback of the technique is that the rate of heat transfer is much lower than in a quench test, hence, high initial specimen temperature is required to cause failure. The high initial temperature introduces the complexities of radiation heat transfer and temperature dependent material properties. A further drawback is that in the reported studies the convection heat transfer coefficient was calibrated by subjecting a pre-cracked disc (with known fracture toughness) to thermal shock and back-calculating convection. Thus, a circular argument was used to make failure predictions.

The liquid metal quench [14, 15] involves immersion of the heated specimen into a lower temperature

0022–2461/92 $03.00 + .12

liquid metal bath. The dominant mode of heat transfer has been shown to be conduction, thus eliminating the temperature dependence of the convection thermal boundary condition. The maximum stress in the specimen is a simple function of the elastic constants of the specimen material and the ratio of the thermal conductivities, densities and specific heats of the specimen and liquid metal. The primary drawbacks are those of other quench tests: stress concentrations occur at corners of specimens, the onset of fracture is not well defined, transient specimen temperature and stress are assumed rather than measured. Furthermore, the liquid metal quench medium may affect crack propagation and is a health hazard.

The contact technique discussed in the present paper addresses many of the problems of previous thermal shock tests. The technique provides controlled thermal boundary conditions and a high rate of heat transfer. It allows for quantitative measurement of the specimen response. Transient specimen temperature is measured continuously and used to calibrate the parameters for the thermal boundary condition. Time-to-failure during the thermal shock is measured using acoustic emission. The technique lends itself to validation of theoretical models of thermal stress fracture of ceramics because each step of the model can be investigated separately. Failure predictions are based on thermal and mechanical parameters which are established independently of the thermal shock test. A direct comparison can be made between failure in thermal shock and failure in mechanical loading because the same flaw population controls strength in both tests. The present study compares experimental results using a soda-lime glass with theoretical predictions based on a finite element thermal stress analysis combined with a statistical theory of fracture.

2. Statistical theory of fracture

Early work on thermal shock in ceramics recognized the advantages of applying Weibull's statistical theory of fracture to failure under thermal stress conditions [16]. A statistical approach simultaneously describes scatter in test results and accounts for the effects of volume and multi-axial stress on strength. The Batdorf formulation of the statistical theory of fracture for arbitrary fracture criterion [17, 18] has been applied previously to the air jet thermal shock tests [13] and the water quench test [19].

The general expression for the failure probability distribution of a brittle material under an arbitrary multi-axial stress distribution is given by [19–21]

$$P = 1 - \exp\left\{ -\left[\frac{1}{m}!\right]^m \frac{1}{v} \int_V \left(\frac{\sigma_1}{\sigma_v}\right)^m G(m, s, t)\, dV \right\} \quad (1)$$

where s and t are the ratios of the ordered principal stresses $\sigma_1 \geq \sigma_2 \geq \sigma_3$,

$$s = \frac{\sigma_2}{\sigma_1}, \quad t = \frac{\sigma_3}{\sigma_1} \quad (2)$$

m is the Weibull modulus, V the volume of the body, and σ_v is the mean uniaxial tensile strength of a unit volume, v. The function G depends on the stress state and the fracture criteria. In uniaxial tension $G = 1$ and the standard Weibull distribution is obtained. The term including the factorial function is used to assure that σ_v is the arithmetic mean stress [22]. Equation 1 represents the probability of failure of a specimen under given stress state where fracture originates with a volumetric flaw. The primary advantage of this representation of the distribution function in Equation 1 is that the σ_v does not depend on the type of test, whether a tensile, bend or biaxial test. The probability of failure due to surface flaws is determined by evaluating Equation 1 over the surface of the body with σ_s, the mean strength of unit surface area, replacing σ_v. In most cases the surface stresses and flaws dominate over volume stresses and flaws.

For an isotropic homogeneous material, considering only failure due to tensile stresses, and applying the Batdorf shear insensitive flaw fracture criterion, the function G is given explicitly by the series [23]

$$G(m, s, t) = \frac{(m!)^2}{(2m)!} \sum_{i,j,k}^{m} \frac{(2i)!(2j)!(2k)!}{(i!j!k!)^2} s^j t^k \quad (3)$$

where i, j, k are positive integers satisfying $0 \leq i, j, k \leq m$, and $i + j + k = m$. Under conditions of equiaxial stress, Equation 3 can be approximated by the function [23]

$$G(m, 1, 0) \approx m^{0.45} \quad (4)$$

The previous discussion was developed to describe failure of brittle materials under mechanical loading. Under thermal shock loading a statistical model of fracture must also consider the effects of decreasing stress [24]. For example, in a thermal shock test the stresses exhibit a peak at some time and then decrease at later time, however the cumulative failure probability does not decrease with time. When the stress in any element of a body is not monotonically increasing, it is necessary to retain the maximum failure probability of that element for all subsequent time.

Equations 1 and 3 were integrated into a finite element analysis computer program [25]. The failure probability of a particular static or transient stress state is calculated using the thermal and mechanical boundary conditions, the thermal and mechanical material properties, and the statistical strength parameters.

3. Experimental procedure

3.1. Materials

The material used in the present study is a soda-lime silicate plate glass whose temperature dependent properties and their estimated uncertainties are listed in Table I [26]. One hundred and fifty, 5.08 cm diameter discs were cut from 20.3 cm × 25.4 cm × 0.159 cm glass sheets using a glass hole-cutting tool. The edges of the discs were ground to make handling safer. The discs were cleaned and annealed at 528 °C to relieve residual stresses. The prepared specimens were numbered and randomized using a 'pick them from a hat' type algorithm.

TABLE I Specimen dimensions, temperature dependent thermal and mechanical properties of soda-lime glass discs

	Temperature (°C)	Soda-lime glass
Disc radius, a (cm)	23	2.46
Disc thickness, d (cm)	23	0.19 ± 0.002
Thermal conductivity, k ($W\,cm^{-1}\,°C^{-1}$)	23	0.010 ± 0.001
	200	0.0105
	400	0.014
Density, ρ ($g\,cc^{-1}$)	23	2.5 ± 0.05
Specific heat, c ($Wg^{-1}\,°C^{-1}$)	23	0.80 ± 0.05
	200	1.00
	400	1.13
Young's modulus, E (GPa)	23	69 ± 5
	200	67
Poisson's ratio, ν	23	0.25
Thermal expansion coefficient, α ($\times 10^{-6}\,°C^{-1}$)	23	9.1 ± 0.2
	200	9.3
	400	11

3.2. Concentric ring flexure test

Strength parameters of the glass discs were measured in biaxial flexure using a concentric ring [27, 28] loading fixture designed for the present study. The inner and outer spans of the concentric rings were 2.22 and 4.76 cm, respectively. Failure load was measured using a universal testing machine at a crosshead speed of 100 mm min^{-1}.

3.3. Contact thermal shock test

A schematic diagram of the metal rod contact thermal shock apparatus is shown in Fig. 1. Thermal shock occurs when the centre of the heated disc specimen is placed in contact with the brass cooling rod. The rapid cooling and contraction of the centre of the specimen results in uniform equi-biaxial tensile thermal stress.

A statistically significant number of soda-lime glass specimens were tested at each initial temperature of 400, 450, 500, and 550 °C. Groups of eight specimen-firebrick holder assemblies were heated at a rate of approximately 2 °C min^{-1} in a box furnace. The specimen temperature was monitored with a thermocouple located between the top surface of the specimen and the refrasil insulation layer. After holding for 30 min at the desired initial temperature (within ± 5 °C) the specimen holder assembly was removed from the furnace and placed at room temperature on a stand above the 2.5 cm diameter brass cooling rod. The assembly was lowered at a steady uniform rate on to the cooling rod with the aid of mechanical guides. Alignment of the brass rod with the centre of the disc specimen was within 2 mm. A thin layer of a light oil was applied over the end of the brass rod in order to reduce the thermal contact resistance and increase the rate of heat transfer. The transient temperature of the centre of the backside of the specimen was recorded using a thermocouple and data acquisition system.

3.4. Acoustic emission

Acoustic emission has been used to detect the initiation of cracking in water quench test [19, 29]. Signals due to cracking events were detected by immersing a broad-band ultrasonic transducer in the water bath. Boiling was found to generate low frequency noise which can mask the desired fracture event signals. This technique demonstrated that damage can be introduced at thermal shocks well below the critical temperature difference [30].

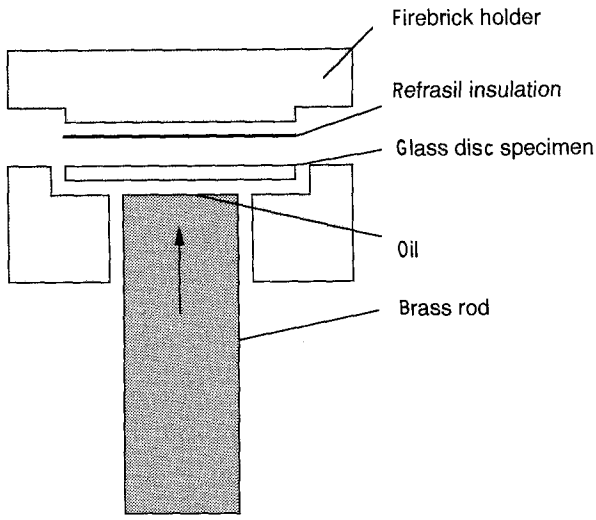

Figure 1 Brass rod contact thermal shock apparatus.

The present study employed the apparatus shown in Fig. 2 to measure time-to-failure in the contact thermal shock test. A broad-band piezoelectric transducer was placed in contact with the bottom of the brass rod with a layer of acoustic couplant. The transducer was connected to a 40 dB pre-amplifier, an active low pass filter (5 kHz cut-off), and an analogue-to-digital (A/D) converter card in a microcomputer. The highest frequency at which acoustic emission events could be measured was 5 kHz with the maximum sample rate of 12 000 samples s^{-1} using a single channel. The dominant frequencies of acoustic emission from fracture events in ceramics are over 100 kHz, however the signals detected at frequencies below 5 kHz were adequate to establish the time-to-failure. Indeed, the primary fracture event was audible. Time-to-failure was measured as the time difference between the signal produced by contact of the rod with the specimen and the first fracture event signal.

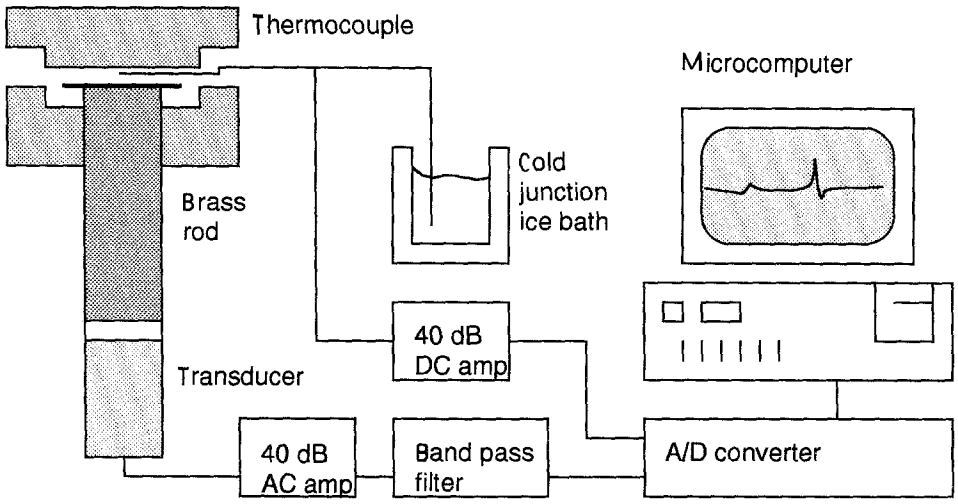

Figure 2 Apparatus used to measure time-to-failure and specimen temperature in the contact thermal shock test.

4. Results and discussion

4.1. Concentric ring flexure

Two groups of soda-lime glass specimens were tested in concentric ring flexure: those in the original condition and those which survived the contact thermal shock test. Table II summarizes the statistical strength parameters.

The maximum stresses in concentric ring flexure are uniform equi-biaxial over the tensile surface in the region beneath the loading ring. The radial and tangential components of stresses are given by [31]

$$\sigma_r = \sigma_\theta = \frac{3L}{4\pi d^2}\left\{2(1+\nu)\ln\frac{a}{r_0} + (1-\nu) \times\left[1-\left(\frac{r_0}{a}\right)^2\right]\right\}, \quad r \leq r_0 \tag{5}$$

where L is the applied load, r_0 is the inner loading ring radius, a is the outer support ring radius, and d is the disc thickness. The failure probability distribution under this stress state is calculated by evaluating Equation 1 over the surface of the disc. If the stresses outside of the inner loading ring are neglected then Equations 1, 4, and 5 yield

$$P = 1 - \exp\left\{-\left(\frac{1}{m}!\right)^m \frac{1}{s} A\left(\frac{\sigma_{ring}}{\sigma_s}\right)^m m^{0.45}\right\} \tag{6}$$

where $A = \pi r_0^2$ is the stressed surface area and σ_s is used in place of σ_v.

The parameters m and σ_s were calculated from a linear regression of Equation 6 using the strength measurements and the failure probability. These values are listed in Table II. Fig. 3 shows the strength distributions of the two groups of specimens. The Weibull distribution function was fit to the specimens in the original condition. It is evident that the thermal shock cycle only slightly increased the mean strength of the survivors.

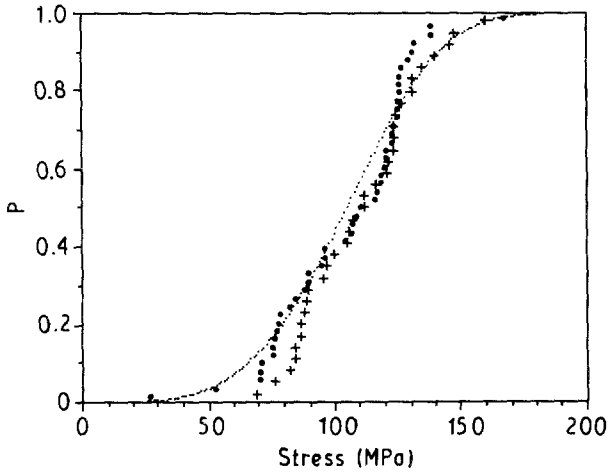

Figure 3 Strength of glass discs tested in concentric ring flexure, including specimens in: (●) original condition; (+) thermal shock survivors, and (· · · ·) Weibull distribution function for mean strength of 105 MPa and Weibull modulus of 4.

4.2. Contact thermal shock

Table III summarizes the results of the contact thermal shock tests. As expected the higher initial specimen temperatures caused a larger fraction of the

TABLE II Summary of concentric ring flexure test results

	Original condition	Shock survivors
Number of specimens, N	47	33
Mean fracture load, L (N)	632	665
Standard deviation of load (N)	161	138
Mean fracture stress, S (MPa)	104	110
Standard deviation of stress (MPa)	26	23
Weibull modulus, m	4	5
Mean strength of unit surface area (cm^2), σ_s (MPa)	174	

TABLE III Summary of brass rod thermal shock results for soda-lime glass discs: initial temperature, number of samples tested, number that failed, total probability of failure of the cycle, and calibrated convection coefficient

Initial temperature (°C)	400	450	500	550
Number tested	32	24	18	16
Number failed, J	8	12	16	16
Probability of failure, P_{tot}	0.25	0.50	0.89	1.0
Calibrated h (W cm^{-1} °C^{-1})	0.11	0.14	0.16	0.20

specimens to fail. The fraction of the specimens that failed with a given initial temperature is the total probability of failure of the thermal stress cycle, P_{tot}. Micrographs of specimens after failure in the thermal shock test and the concentric ring test are shown in Fig. 4. In both tests cracks initiate in the centre and propagate outward. In the thermal shock the cracks curve and arrest due to the compressive stresses in the outer region of the disc. Specimens that fail after short time (with high initial temperature) exhibit more cracking than those that fail after a longer time (with low initial temperature).

Fig. 5 shows a typical acoustic signal monitored during the contact thermal shock. At $t = 0$ the trace is triggered by the sound produced by contact between the specimen and rod. At some later time, the time-to-failure, a very distinct peak due to fracture initiation is evident. In some cases additional fracture events were observed after the primary event.

The finite element method analysis of the temperature and stress employed the temperature-dependent

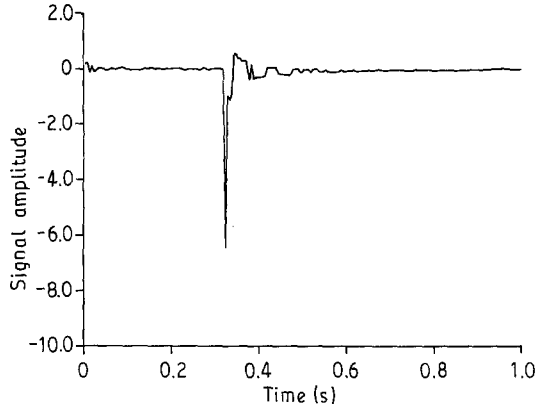

Figure 5 Typical acoustic emission signal from the contact thermal shock test.

thermal and mechanical properties listed in Table I. Heat conduction between the brass rod and the disc specimen was not perfect; the thermal contact resistance was modelled as a convective heat transfer boundary condition. This is justified because the conductivity of the brass rod is so much higher than that of the glass that the temperature of the brass rod does not change appreciably during the course of the test. The convective heat transfer coefficients, h, at each initial temperature, listed in Table III, were chosen such that the finite element analysis prediction of the time variation of the temperature of the backside of the specimen agreed with the experimental measurements.

Fig. 6 shows the finite element analysis prediction of the maximum tensile radial surface stress as a function

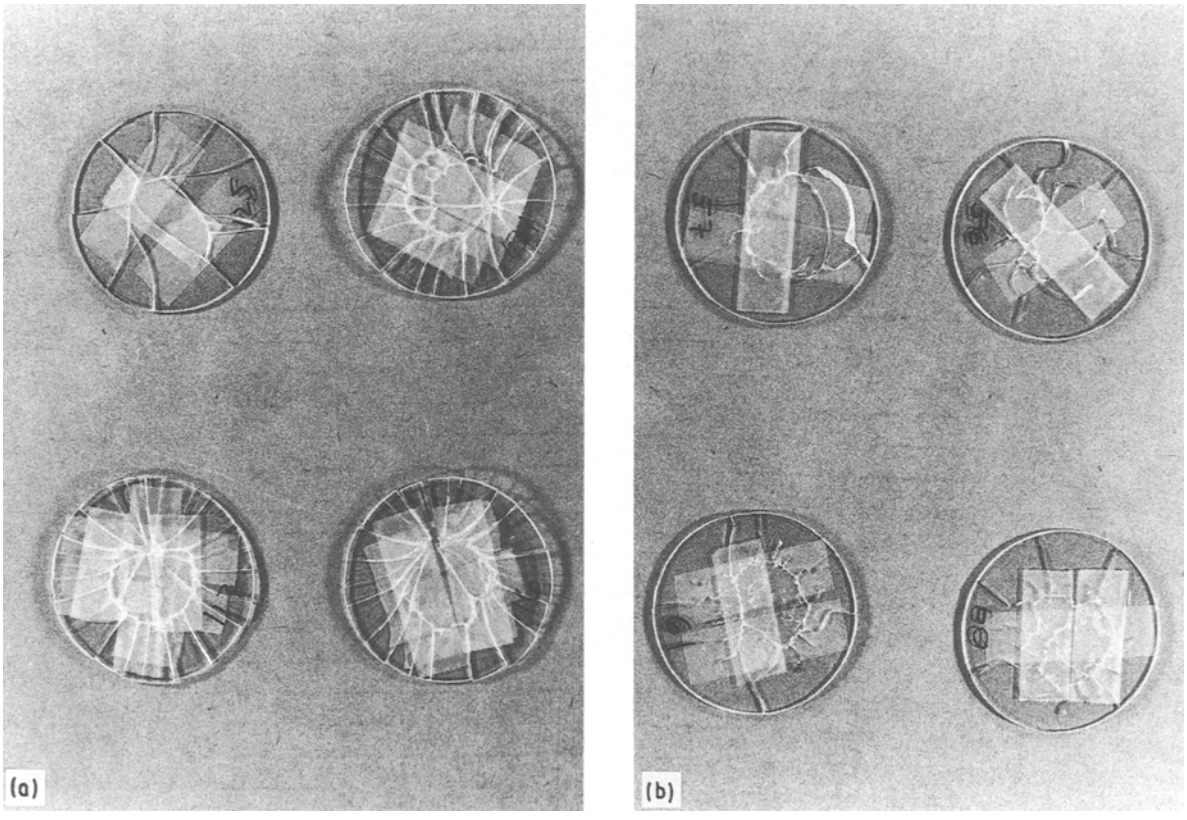

Figure 4 Micrograph of typical specimens tested in (a) the concentric ring test and (b) the contact thermal shock test.

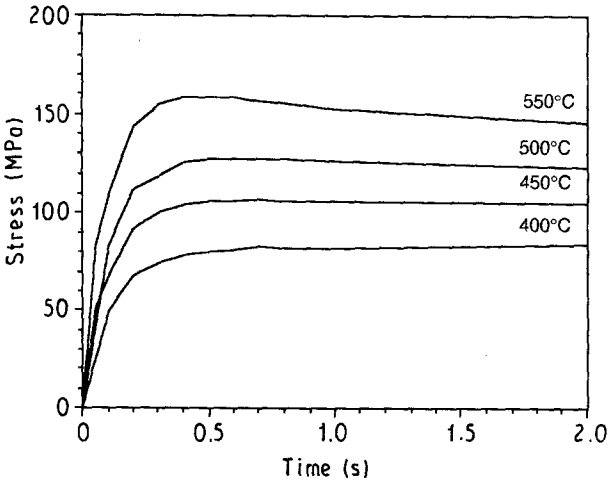

Figure 6 Surface radial stress as a function of time and initial disc temperature in the contact thermal shock test. Calculated using a finite element analysis.

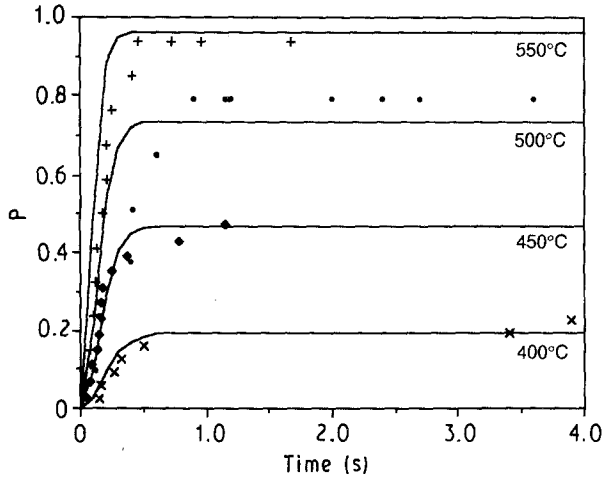

Figure 7 Experimental results and theoretical curves showing failure probability of glass discs as a function of time with various initial specimen temperatures. (symbols show experimental results.)

of time for various values of initial specimen temperature. Stresses are essentially equi-biaxial; the tangential component of surface stress is similar to the radial. Stresses in the thickness direction are negligible. At small values of time (< 0.5 s) the stresses are confined to the contact surface and at larger values of time (> 2 s) the stresses are more uniform through the thickness of the disc. Surface stresses control the fracture behaviour in thermal shock for two reasons: maximum stresses occur at small values of time, and surface flaws dominate over volume flaws in glass. The uniform equi-biaxial stress state in the contact thermal shock is very similar to the stress state in the concentric ring test. Hence, the same surface flaw population is sampled in both tests and a direct comparison of failure modes can be made.

Given the stress distribution the theoretical probability of failure at each instant of time was calculated with the aid of Equation 1 evaluated over the surface of the specimen. If stresses outside the contact area are neglected an approximate solution is given by Equation 6 using the surface stress shown in Fig. 6. Fig. 7 compares the theoretical predictions of time-to-failure with the experimental measurements. The probability of failure P_j was assigned to each measured time-to-failure in the following manner. The magnitude of the stress S_j was calculated by finite element analysis (FEA) at each value of the time-to-failure. These stresses were ranked and assigned a probability of failure according to

$$P_j = P_{tot} \frac{j - 0.3}{J + 0.4} \quad (7)$$

were P_{tot} is the probability of failure of the cycle (listed in Table III), j is the rank, and J is the number of samples that failed with that initial specimen temperature. Values of time-to-failure larger than 1 s indicate delayed failure under constant stress, characteristic of glass.

Note that in Fig. 6 with initial temperature of 550 °C the radial surface stress exhibits a maximum near 0.5 s. As discussed in the introduction, the statistical model requires that the probability of failure

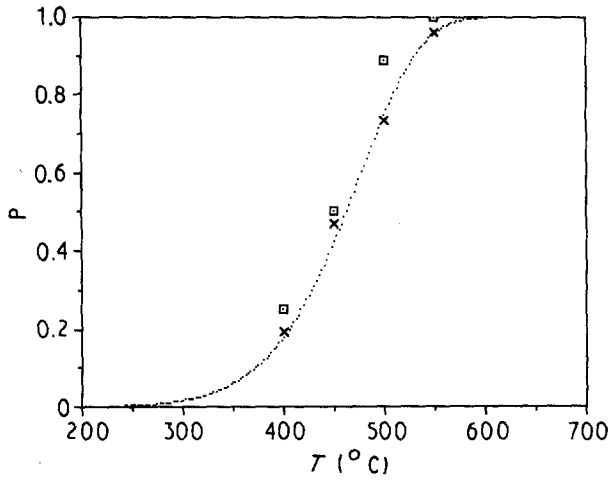

Figure 8 Experimental results (⊡), theoretical results (×), and Weibull curve fit (····) to theoretical results showing probability of failure of glass discs as a function of initial specimen temperature.

associated with these surface elements must be retained at all subsequent values of time as the stress decreases.

Fig. 8 shows failure probability P_{tot} as a function of initial specimen temperature. Comparison is made between the experimental measurements, the finite element analysis results and a Weibull distribution curve fit to the theoretical results. The agreement between theory and experiment in Figs 7 and 8 is within the uncertainty of the material parameters and the experimental measurements. Both the time-to-failure and the overall failure probability are well described by the statistical model of thermal stress fracture.

5. Conclusion

The contact thermal shock test offers several advantages over traditional thermal shock tests: well defined thermal boundary conditions, high rate of heat transfer, measurement of transient specimen temperature, and measurement of time-to-failure using acoustic emission. The technique is demonstrated with

soda-lime glass and a range of initial specimen temperatures. Experimental results are compared to predictions of a model of thermal stress fracture of ceramic materials based on a finite element thermal stress analysis combined with a statistical theory of fracture. The analysis uses the material's thermal and mechanical properties, the thermal and mechanical boundary conditions, and the material's statistical strength parameters obtained from concentric ring flexure tests. The statistical model of thermal stress fracture is found to accurately describe the statistical distribution of experimental measurements of time-to-failure and overall probability of failure during the contact thermal shock test.

Acknowledgement

This study was supported by the National Aeronautics and Space Administration under Grant No. NAGW 199.

References

1. W. R. BUESSEM, *J. Amer. Ceram. Soc.* **38** (1955) 15.
2. W. D. KINGERY, *ibid.* **38** (1955) 3.
3. R. W. DAVIDGE and G. TAPPIN, *Trans. Br. Ceram. Soc.* **66** (1967) 405.
4. D. P. H. HASSELMAN, *J. Amer Ceram. Soc.* **53** (1970) 490.
5. J. P. SINGH, Y. TREE and D. P. H. HASSELMAN, *J. Mater. Sci.* **16** (1981) 2109.
6. P. F. BECHER, *J. Amer. Ceram. Soc.* **64** (1981) C17.
7. P. F. BECHER, D. LEWIS, K. R. CARMAN and A. C. GONZALEZ, *Amer. Ceram. Soc. Bull.* **59** (1980) 542.
8. D. LEWIS, *J. Amer. Ceram. Soc.* **63** (1980) 713.
9. D. LEWIS, in "Fracture Mechanics of Ceramics," Vol. 6, (Plenum, New York, 1983) pp. 487–96.
10. M. ISHITSUKA, T. SATO, T. ENDO and M. SHIMADA, *J. Mater. Sci.* **24** (1989) 4057.
11. K. J. KONSZTOWICZ, *J. Amer. Ceram. Soc.* **73** (1990) 502.
12. K. T. FABER, M. D. HUANG and A. G. EVANS, *ibid.*, **64** (1981) 296.
13. J. R. BROCKENBROUGH, L. E. FORSYTHE and R. L. ROLF, *ibid.* **69** (1986) 634.
14. H. HENCKE, J. R. THOMAS and D. P. H. HASSELMAN, *ibid.*, **67** (1984) 393.
15. M. OGUMA, C. J. FAIRBANKS and D. P. H. HASSELMAN, *ibid.*, **69** (1986) C87.
16. S. S. MANSON and R. W. SMITH, *ibid.* **38** (1955) 18.
17. S. B. BATDORF, in "Fracture Mechanics of Ceramics," Vol. 3, (Plenum, New York, 1978) pp. 1–30.
18. S. B. BATDORF and H. L. HEINISCH, *J. Amer. Ceram. Soc.* **61** (1978) 355.
19. W. P. ROGERS, A. F. EMERY, R. C. BRADT and A. S. KOBAYASHI, *ibid.* **70** (1987) 406.
20. W. P. ROGERS, *Int. J. Fract.*, in press.
21. W. P. ROGERS, PhD thesis, University of Washington, Seattle (1987).
22. P. STANLEY, H. FESSLER and A. D. SIVILL, *Proc. Br. Ceram. Soc.* **22** (1973) 453.
23. S. B. BATDORF, *Int. J. Fract.*, **13** (1977) 5.
24. P. STANLEY and F. S. CHAU, *Proc. Br. Ceram. Soc.* **32** (1982) 119.
25. A. F. EMERY, in "FLIP: Finite element analysis package," University of Washington, 1987.
26. N. P. BAUSAL and R. H. DOREMUS, in "Handbook of Glass Properties," (Academic Press, London, 1986).
27. J. E. RITTER, K. JAKUS, A. BATAKIS and N. BANDYOPADHYAY, *J. NonCryst. Sol.* **38&39** (1980) 419.
28. J. B. WACHTMAN, W. CAPPSS and J. MANDEL, *J. Mater. Sci.* 7 (1972) 188.
29. A. G. EVANS, M. LINZER and H. JOHSON, *ibid.* **10** (1975) 1608.
30. K. J. KONSZTOWICZ and D. FONTAINE, *J. Nondestruct. Eval.* **8** (1989), 1.
31. R. J. ROARK and W. C. YOUNG, in "Formulas for Stress and Strain," 5th Ed. (McGraw-Hill, New York, 1982) p. 362.

Received 21 August 1990
and accepted 28 February 1991